

D. K. Hall¹

Gas Turbine Laboratory,
Department of Aeronautics and Astronautics,
Massachusetts Institute of Technology,
Cambridge, MA 02139
e-mail: dkhall@mit.edu

E. M. Greitzer

Gas Turbine Laboratory,
Department of Aeronautics and Astronautics,
Massachusetts Institute of Technology,
Cambridge, MA 02139

C. S. Tan

Gas Turbine Laboratory,
Department of Aeronautics and Astronautics,
Massachusetts Institute of Technology,
Cambridge, MA 02139

Analysis of Fan Stage Conceptual Design Attributes for Boundary Layer Ingestion

This paper describes a new conceptual framework for three-dimensional turbomachinery flow analysis and its use to assess fan stage attributes for mitigating adverse effects of inlet distortion due to boundary layer ingestion (BLI). A nonaxisymmetric throughflow analysis has been developed to define fan flow with inlet distortion. The turbomachinery is modeled using momentum and energy source distributions that are determined as a function of local flow conditions and specified blade camber surface geometry. Comparison with higher-fidelity computational and experimental results shows the analysis captures the principal flow redistribution and distortion transfer effects associated with BLI. Distortion response is assessed for a range of (i) design flow and stagnation enthalpy rise coefficients, (ii) rotor spanwise work profiles, (iii) rotor–stator spacings, and (iv) nonaxisymmetric stator geometries. Of the approaches examined, nonaxisymmetric stator geometry and increased stage flow and stagnation enthalpy rise coefficients provide the greatest reductions in rotor flow nonuniformity, and may offer the most potential for mitigating performance loss due to BLI inlet distortion. [DOI: 10.1115/1.4035631]

1 Introduction

In this paper, we present an analysis of axial fan stage behavior with inlet distortion from boundary layer ingestion (BLI). It is well known that BLI, i.e., having a portion of an aircraft's boundary layer pass through the propulsor, so that propulsive power is added to the flow at a lower average velocity, decreases the excess kinetic energy in the downstream jet and increases propulsive efficiency, potentially reducing aircraft fuel burn [1–4]. Two recent BLI aircraft concepts are the Cambridge-MIT Silent Aircraft [5] and the D8 “double bubble” aircraft, developed as part of the NASA N+3 research program to reduce environmental impacts of aviation [6,7]. The D8 has also been assessed in low-speed wind tunnel experiments, where direct comparison of powered models in BLI and non-BLI configurations showed the former gave reductions in required propulsive power of up to 10% [8]. A challenge presented by BLI, however, is the nonuniform stagnation pressure (i.e., stagnation pressure distortion) entering the propulsion system, with the possibility of decreased component efficiency, reduced fan and compressor stall margin, and increased unsteady forces on rotating turbomachinery.

The aerodynamic response of propulsors to inlet distortion has received much attention; an introductory review is given by Longley and Greitzer [9]. Fans and compressors attenuate stagnation pressure distortions, and there is an upstream circumferential flow redistribution that accompanies this attenuation. There is also a strong interaction that can exist between rotor, stator, and downstream components due to the radius scale interaction lengths. These effects have been well described for two-dimensional flows [10,11], and some of the ideas will be used here to give insight into the response to BLI distortion. It will be seen, however, that there are features of the low hub-to-tip ratio turbomachines that typify aeroengine fans that require a three-dimensional flow description.

There has been recent computational work on BLI fan stage performance, including description of the design of a distortion-tolerant BLI fan stage, with estimates of reductions in stage efficiency of 1–2% relative to uniform flow [12]. Other

computational and experimental analyses have found similar efficiency reductions for different geometries [13,14]. Gunn and Hall have shown that fan stage performance depends strongly on three-dimensional flow redistribution upstream of the fan and through the rotor, and that stage efficiency is linked to circumferential flow nonuniformities, particularly local diffusion factor. A useful finding from comparison of calculations for incompressible and transonic flow is that although the details of the flow change between the two (e.g., the occurrence of shocks in the latter regime), the overall features of flow redistribution that determine changes in stage efficiency with inlet distortion are not sensitive to Mach number [14].

The objective of the present work is to determine fan stage attributes that mitigate the effects of inlet distortion on performance. The stagnation pressure distributions considered are representative of inlet distortion for BLI aircraft with short, low-offset inlets such as the D8 [7]. The framework described, however, can be applied to different nonaxisymmetric turbomachinery flow distortions [15]. The focus is on *design point aerodynamic efficiency*; stability and aeromechanics are mentioned in passing but are beyond the scope of this paper.

We emphasize that the problem is treated at the *conceptual level*, which includes the specification of design point flow coefficient and spanwise distribution of stagnation enthalpy rise coefficient (i.e., velocity triangles), axial location of the rotor and stator, and mean camber line. *Knowledge of blade profile*, which is obtained later in the design process, is *not required*. The intent is not to develop a detailed design methodology for BLI propulsors, but rather to *identify conceptual design attributes* that provide favorable conditions for fan stage operation with distortion.

We assess the effect of design choices on BLI fan performance using a newly developed nonaxisymmetric turbomachinery throughflow analysis. The basic idea is to replace the three-dimensional blade geometry with momentum and energy source distributions that generate the flow turning and pressure rise of the turbomachinery [16]. Such analyses have been used to assess the effect of flow nonuniformities on multistage compressor stability [17], fan aerodynamic performance [18], and fan aeroacoustics [19]. Unlike these previous analyses, however, in which the source distributions are extracted from single-passage flow solutions, in the current approach the sources are determined as a function of local flow conditions and an approximate blade geometry, so additional *a priori* flow calculations are not needed.

¹Corresponding author.

Contributed by the International Gas Turbine Institute (IGTI) of ASME for publication in the JOURNAL OF TURBOMACHINERY. Manuscript received December 5, 2016; final manuscript received December 9, 2016; published online March 7, 2017. Editor: David Wisler.

The flow is taken to be inviscid, which is appropriate because, as will be seen, the mechanisms that determine the fan distortion response are inviscid. Blade performance metrics such as diffusion factor can be used as surrogates for assessing efficiency. The model flow is also taken to be incompressible, which simplifies the analysis and is appropriate in light of the findings of Gunn and Hall [14] regarding the small effects of Mach number of fan flow redistribution.

The paper is organized as follows. We first provide a description of the nonaxisymmetric throughflow analysis. We then present comparisons of the analysis with results of higher-fidelity calculations and experiments on BLI fan flow. These illustrate the degree to which the relevant distortion-fan interactions are captured, and hence the utility of the analysis. Third, we determine the effectiveness of different design features by assessing their impact on the magnitude of circumferential flow nonuniformities. Finally, based on the results, we discuss the attributes that have the greatest potential to mitigate the impact of BLI inlet distortion on fan stage performance.

2 Nonaxisymmetric Throughflow Analysis

In this section, we describe the three-dimensional throughflow analysis. The basic concept is shown in Fig. 1, which illustrates a fan rotor geometry and its representation in an equivalent model flow. In the latter, the bladed region is replaced with an axisymmetric fluid volume over the meridional extent of the blade row. Within the volume, momentum and energy source distributions generate flow turning, pressure rise, and enthalpy rise produced by the actual geometry in a pitchwise-averaged sense. The source distributions are defined as a function of local flow conditions and a specified blade camber surface geometry. For uniform inlet conditions, the source distribution generates an axisymmetric flow field equivalent to the circumferential average of the actual flow. For nonaxisymmetric flow, the source distribution is circumferentially nonuniform and generates the appropriate distortion transfer across the blade row.

2.1 Source Term Formulation

2.1.1 Equations of Motion. The description here is presented in terms of inviscid flow. There is no bar to including viscous effects, but it will be seen that an inviscid description is adequate to capture the relevant flow mechanisms for the problem of interest. For steady flow, the local momentum and energy source terms are represented as a body force per unit mass \mathbf{f} and an energy addition rate per unit mass \dot{e} . The equations of conservation of mass, momentum, and energy, including the source terms, are

$$\nabla \cdot (\rho \mathbf{V}) = 0 \quad (1)$$

$$\mathbf{V} \cdot \nabla \mathbf{V} + \frac{1}{\rho} \nabla p = \mathbf{f} \quad (2)$$

$$\mathbf{V} \cdot \nabla h_t = \mathbf{V} \cdot \mathbf{f} + \dot{e} \quad (3)$$

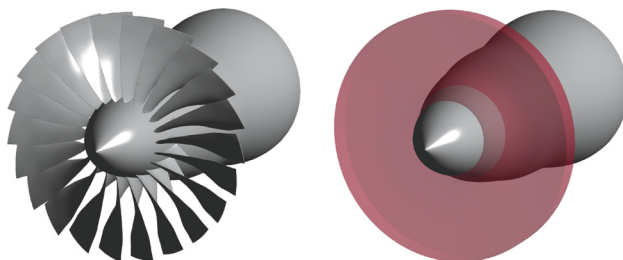


Fig. 1 Comparison of three-dimensional fan rotor geometry and source distribution volume for equivalent model flow

Equations (1) and (2) are sufficient for incompressible flow, but the general compressible case including Eq. (3) is considered here to define the relationship between the source terms and the stagnation enthalpy and entropy, corresponding to work addition and losses, respectively. The stagnation enthalpy change along a streamline is zero except in rotating blade rows, where it is related to the changes in swirl velocity due to the circumferential force

$$\mathbf{V} \cdot \nabla h_t = (\Omega r) f_0 \quad (4)$$

Equation (4) is the differential form of the Euler turbine equation for the model flow. The energy source, \dot{e} , corresponds to entropy generation in the model flow

$$T \mathbf{V} \cdot \nabla s = \dot{e} \quad (5)$$

Combining Eqs. (3)–(5), the entropy generation is related to the body force component in the relative streamwise direction

$$T \mathbf{V} \cdot \nabla s = -\mathbf{W} \cdot \mathbf{f} \quad (6)$$

where $\mathbf{W} = \mathbf{V} - (\Omega r) \hat{\theta}$ is the velocity in the blade-relative frame.

Equation (6) shows the usefulness of characterizing the momentum source in terms of components parallel and normal to the relative direction. Entropy is generated in the model flow by a parallel force acting opposite to the streamwise direction in the relative frame and corresponding energy source, \dot{e} , to satisfy Eq. (5) [20]. The force normal to the relative flow direction generates reversible flow turning. Near the design point of axial turbomachines, the contribution of the parallel force to flow turning, pressure rise, and enthalpy rise is much smaller than the normal force, and we neglect it in the current description, consistent with the assumption of inviscid flow.

2.1.2 Blade Loading Model. The source term distribution is defined as a function of local flow conditions and an approximate blade geometry, characterized at this conceptual stage by a blade camber surface normal distribution, $\hat{\mathbf{n}}(x, r)$. Figure 2 shows the geometry of the local blade camber surface normal and tangent plane, relative velocity vector, and normal force vector.

The momentum source per unit mass, \mathbf{f} , is modeled as a blade force that scales with the square of the local relative velocity and the deviation angle δ between the blade tangent surface and the relative velocity vector, distributed uniformly over one blade pitch. The direction of \mathbf{f} is normal to the relative streamwise direction and in the plane shared by the local blade normal $\hat{\mathbf{n}}$ and the relative velocity vector, \mathbf{W} , and acts to reduce the local deviation, δ , between relative velocity and blade surface

$$|\mathbf{f}| = \frac{(2\pi\delta) \left(\frac{1}{2} W^2 / |n_0| \right)}{2\pi r / B} \quad (7)$$

$$\mathbf{W} \cdot \mathbf{f} = 0 \quad (8)$$

$$(\mathbf{W} \times \hat{\mathbf{n}}) \cdot \mathbf{f} = 0 \quad (9)$$

$$\text{sign}(\mathbf{f} \cdot \hat{\mathbf{n}}) = -\text{sign}(\mathbf{W} \cdot \hat{\mathbf{n}}) \quad (10)$$

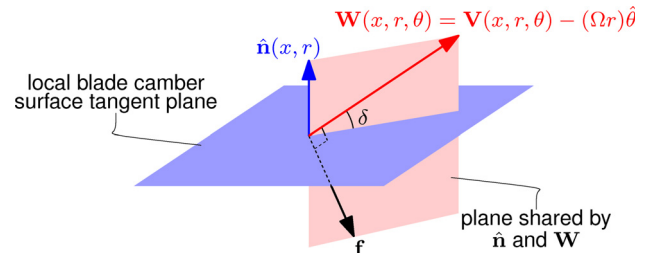


Fig. 2 Geometric description of local blade camber surface normal $\hat{\mathbf{n}}$, relative velocity \mathbf{W} , and momentum source \mathbf{f}

The constant 2π in Eq. (7) yields flat plate airfoil lift ($c_L = 2\pi\delta$) in the low solidity ($s/c \rightarrow \infty$) limit. In the high solidity ($s/c \rightarrow 0$) limit, the flow is everywhere tangent ($\delta = 0$) to the blade camber surface. Equations (3), (4), and (7)–(10) provide closed-form expressions for the source terms as a function of the local flow conditions and specified camber surface normal geometry, and they can therefore be incorporated into numerical solution of the equations of motion.

2.2 Assumptions and Applicability of the Analysis. The nonaxisymmetric throughflow analysis includes several simplifying assumptions. One is that the flow is locally quasi-axisymmetric; in other words, the source terms depend on the local flow conditions, but not on gradients in the circumferential direction. The assumption is appropriate if the characteristic length scale of circumferential nonuniformities is much larger than the blade pitch. This is the case for the geometries considered, which have 20 or more blades, and for BLI inlet distortions whose circumferential length scale is the radius.

A related implication of the distortion circumferential length scale is that unsteadiness in the blade-relative frame can be neglected. The importance of unsteady effects is implied by the reduced frequency, β , which relates the time scales of the flow unsteadiness and the passage throughflow. For distortions with characteristic length scale equal to the radius, β can be approximated in terms of the rotor geometry as

$$\beta = \frac{(c_x/V_x)}{(2\pi/\Omega)} \approx \frac{(\cos \gamma)(1 - r_{\text{hub}}/r_{\text{tip}})}{2\pi\phi A} \quad (11)$$

where γ is the blade stagger, $r_{\text{hub}}/r_{\text{tip}}$ is the blade hub-to-tip ratio, ϕ is the flow coefficient, and A is the blade aspect ratio. For the fan stage geometries considered here, $\beta < 0.1$, and the flow is assumed to be quasi-steady. Comparisons of a source distribution method with full-wheel unsteady Reynolds-averaged Navier-Stokes calculations have shown fan distortion response to be well represented by a steady source distribution flow description [18].

Because we describe the flow in a passage-averaged sense, blade-to-blade features, such as boundary layers, wakes, secondary flows, and tip clearance flow structures, are not resolved. Further, as mentioned previously, because the interest is in behavior near the fan design point, the flow is taken as inviscid, and blade and endwall losses are not included. While these can be added (e.g., nonzero parallel force to represent effects of blade losses), they are not necessary to capture the inviscid redistribution effects which dominate the nonuniform flows examined, as will be seen in Sec. 3.

In summary, the framework we present provides a means of estimating fan stage distortion response without a detailed blade design. The assumption of quasi-steady flow means that steady computational fluid dynamics (CFD) techniques can be used. The source distribution description and the assumption of inviscid flow mean that a relatively coarse grid on an axisymmetric computational domain can be used. The main benefit of the method, however, is the capability to assess the impact of various stage design parameters on propulsor performance before detailed blade design is carried out. This is achieved by using approximate, parametrically defined camber surface distributions which allow manipulation of the radial variations in stage velocity triangles at the design point. The analysis is thus well suited to conceptual level parametric evaluation of distortion response to changes in fan stage design.

3 Fan Stage Distortion Response

We now determine fan stage flow fields with and without distortion using the nonaxisymmetric throughflow analysis we have described. There are two objectives. One is to show, based on comparison of the results with experimental data and with higher-

fidelity computations, that the approximations capture the behavior of fan response to BLI distortion. A second is to identify and describe the features of the flow nonuniformities within the blade rows that lead to decreased performance with inlet distortion.

3.1 Whittle Laboratory BLI Fan Rig. The geometry examined is the low-speed fan stage used in the fan inlet distortion experiments of Gunn et al. [13], Gunn and Hall [14], and Perovic et al. [21]. Design parameters of the fan are listed in Table 1, and a meridional view of the fan stage geometry, computational domain, and the axial measurement planes is given in Fig. 3. The computational domain for the throughflow calculations extends approximately two diameters upstream of the spinner tip and downstream of the stator trailing edge. The rotor and stator camber distributions have been estimated based on radial distributions of leading and trailing edge metal angles [22].

The domain was meshed using POINTWISE [23]. Axisymmetric flow calculations were carried out on a 22.5 deg wedge domain with circumferentially periodic boundary conditions and a butterfly mesh upstream of the spinner. The full-wheel grid consisted of 16 copies of the wedge domain, with grid converged results obtained using 1.8×10^6 cells.

Calculations were performed with ANSYS CFX, a finite volume solver, using the built-in “high-resolution” discretization scheme [24]. Inviscid flow was modeled by solving the laminar Navier-Stokes equations with zero viscosity and slip wall boundary conditions on the hub and casing. The inlet stagnation pressure was fixed, with flow normal to the inlet boundary, and the fan operating point was set by varying the outlet static pressure. Within the rotor and stator regions, momentum and energy sources were calculated, as described above, as a function of the local camber normal and velocity vectors on each solver iteration and added to the equations of motion.

Figure 4 shows a comparison of calculated and measured stage stagnation pressure rise characteristic, as well as the design point stagnation enthalpy rise. The inviscid approximation does not include blade losses, so the stagnation pressure rise and stagnation enthalpy rise coefficients are equivalent. The calculations match the measured stage stagnation enthalpy rise to within 3% at the design point flow coefficient, $\dot{m}/(\rho A_1 U_{\text{mid}}) = 0.5$.

Figure 5 shows the spanwise distributions of pitchwise-averaged rotor inlet and exit axial velocity at the stage design point. The nonaxisymmetric throughflow analysis agrees well with measurements over most of the blade span. The analysis does not capture the rotor tip clearance and endwall flow, but these do not have a large impact on the flow away from the

Table 1 Whittle Laboratory BLI fan rig design parameters

Flow coefficient, $= \dot{m}/(\rho A_1 U_{\text{mid}})$	0.5
Stage work coefficient, $= \Delta h_t/U_{\text{mid}}^2$	0.47
Stage reaction	0.81
Rotor inlet tip Mach number	0.13
Rotor tip Reynolds number	2.0×10^5
Rotor inlet hub-to-tip radius ratio	0.3
Rotor inlet tip diameter (m)	0.5
Number of rotor blades	20
Number of stator vanes	30

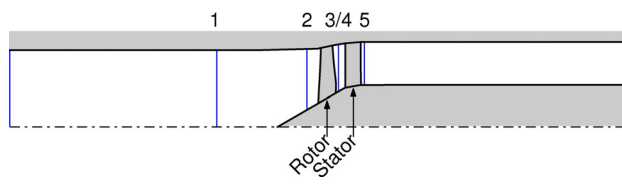


Fig. 3 Meridional geometry of Whittle Laboratory BLI rig computational domain

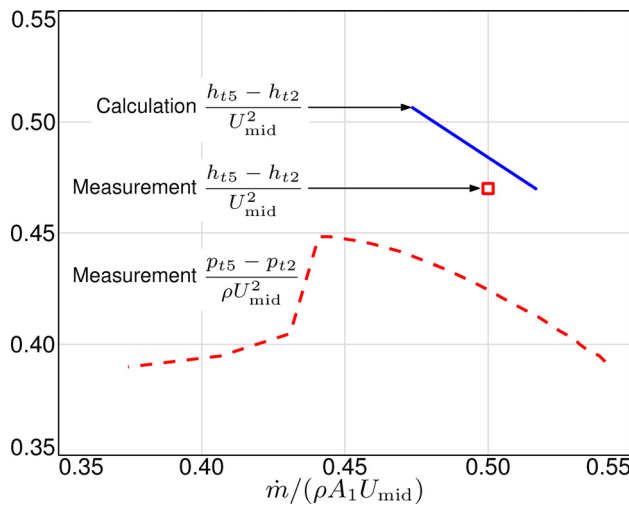


Fig. 4 Stagnation pressure and enthalpy rise characteristics with uniform inlet conditions; comparison of throughflow calculation and measurements [14]

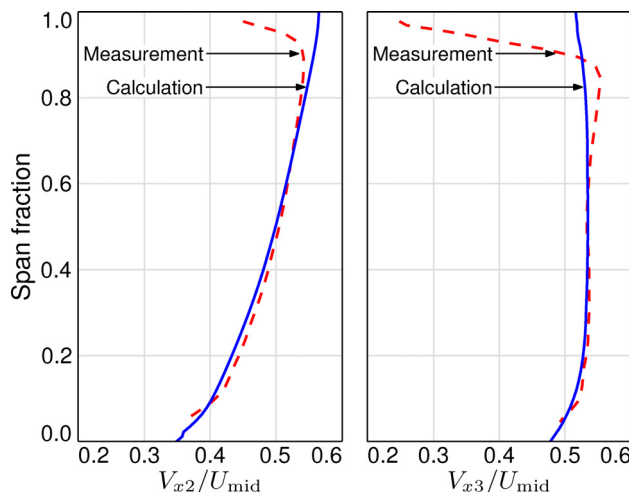


Fig. 5 Spanwise distributions of axial velocity normalized by midspan wheel speed upstream and downstream of the rotor; comparison of throughflow calculation and measurements [14]

endwalls. Further, as seen below and perhaps more importantly, the analysis captures the flow *nonuniformities* near the endwalls with inlet distortion.

3.2 BLI Inlet Distortion. The results from applying the throughflow analysis to the distortion experiments of Gunn and Hall [14] are given below. The inlet stagnation pressure distribution is shown in Fig. 6. The vertically stratified distribution is representative of BLI distortion for the aircraft of interest, which has embedded propulsors with small offset from the fuselage surface and short inlets [7]. There are small (compared to a radius) length-scale variations in the measured stagnation pressure distribution due to the design of the screen used to generate the distortion. These variations are not included in the calculations, consistent with the pitchwise-average representation of the model flow.

3.3 Rotor Flow Field. The conditions at the rotor inlet are set by the upstream redistribution due to interaction between the inlet distortion and the fan. Because of the difference in local pressure rise across the fan and the approximately circumferentially uniform stage exit static pressure, low stagnation pressure

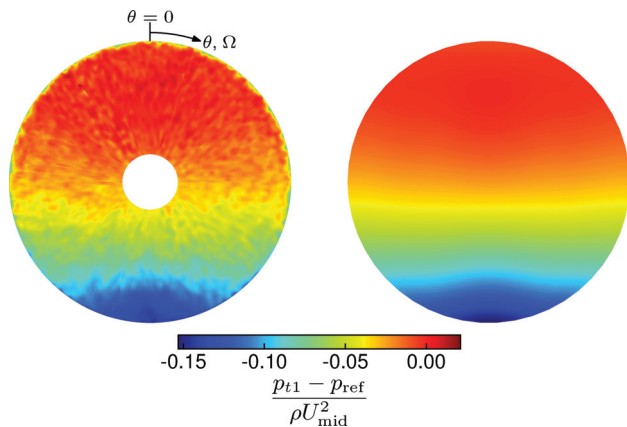


Fig. 6 Inlet stagnation pressure distribution; comparison of measurements [22] (left) and nonaxisymmetric throughflow calculation inlet boundary condition (right)

streamtubes experience greater streamwise acceleration upstream of the fan. The consequences are (i) attenuation of the axial velocity distortion, (ii) a top-to-bottom flow redistribution due to larger streamtube contraction of the low stagnation pressure flow, and (iii) circumferential velocity distortions at the rotor inlet.

Figure 7 shows the comparison of calculated and measured circumferential distributions of rotor inlet (station 2) axial velocity and absolute swirl angle, at 25% and 75% span, at the design point flow coefficient. The small length-scale inlet stagnation pressure variations due to the screen design convect downstream to the rotor inlet, resulting in the rippled velocity distributions observed in the measurements. These are small compared to the peak-to-peak distortion magnitude and do not affect the bulk distortion response behavior.

The axial velocity distortion is larger near the tip than near the hub, because of the spanwise variation in stagnation pressure circumferential nonuniformity. The absolute swirl angles are largest at circumferential locations near $\theta = 90$ deg and $\theta = 270$ deg (measured from $\theta = 0$ deg at the top of the fan, so the minimum upstream stagnation pressure occurs at $\theta = 180$ deg), where the downward component of the velocity is aligned with the circumferential direction, and near the hub, where the downward velocity is increased due to the blockage of the spinner. The difference in axial velocity distortion between 25% and 75% span, as well as the shapes of the circumferential distributions, is well captured.

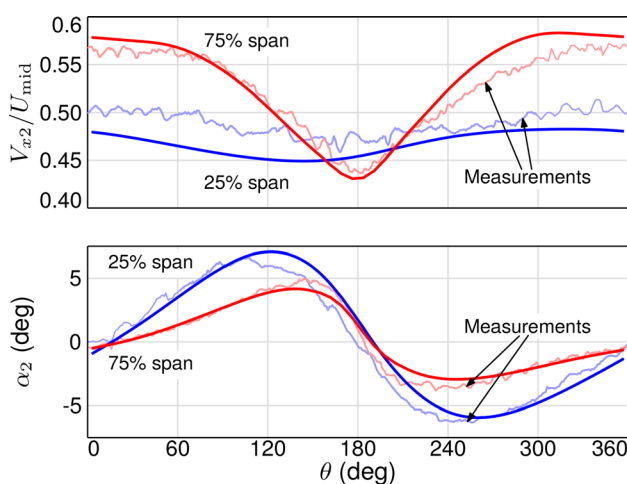


Fig. 7 Circumferential distributions of rotor inlet axial velocity and absolute swirl angle; comparison of nonaxisymmetric throughflow calculation and measurements [14]

The flow far upstream is axial, and the measured rotor inlet swirl, and thus the upstream redistribution, is also described by the nonaxisymmetric throughflow analysis.

The upstream redistribution results in circumferential nonuniformities in rotor relative inlet flow angle, stagnation enthalpy rise, streamtube contraction, and diffusion through the rotor, illustrated in Fig. 8. Figure 8(a) shows the difference between calculated rotor inlet relative flow angle, β_2 , and the circumferential average at that radius, which represents the local incidence angle distortion. For a tip section, the inlet flow angle reaches a maximum near $\theta = 180$ deg, where the stagnation pressure and axial velocity are low, and the absolute swirl angle is near zero (the region labeled A in Fig. 8). For a hub section, the axial velocity distortion is small, and the main impact on incidence angle is the decrease due to coswirl (at B) and increase due to counterswirl (at C). At midspan, variations in both axial and swirl velocity affect the local incidence, but the flow angle distortions are smaller than those near the hub and tip. The peak-to-peak circumferential nonuniformity in incidence angle is largest at the hub, even though the incoming stagnation pressure distortion is smallest there.

Figure 8(b) shows the rotor stagnation enthalpy rise coefficient distribution. The work input exhibits circumferential nonuniformities similar to the incoming relative flow angle in Fig. 8(a), indicating that circumferential variations in incidence angle, and thus flow turning, have a larger effect on work input than velocity nonuniformities. The peak stagnation enthalpy rise occurs at the location of peak rotor tip incidence near region A. The hub has the lowest work input for uniform inlet conditions, and it experiences decreased work input (relative to the circumferential mean) near $\theta = 90$ deg, where the hub incidence is most negative, and increased work input near $\theta = 270$ deg, where the hub incidence is largest, due to the swirl distortion seen at B and C.

The nonuniform work input results in nonuniform streamtube contraction through the blade row, as shown in Fig. 8(c). The

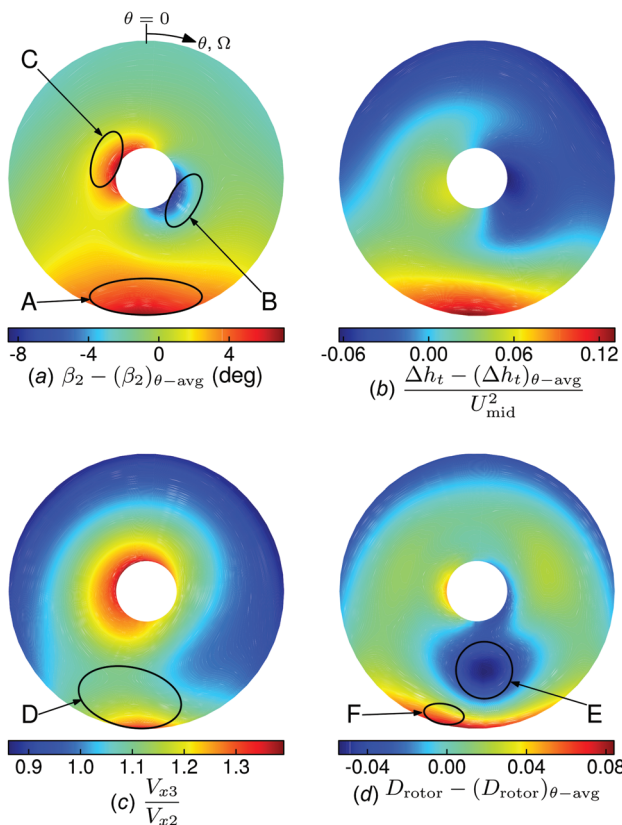


Fig. 8 Calculated rotor inlet relative flow angle distortion (a), stagnation enthalpy rise (b), streamtube contraction (c), and diffusion factor 180 deg (d)

contraction is larger where the work input is high (region D), consistent with observations of radial redistribution between rotor inlet and exit that reduces the axial velocity distortion [14].

Figure 8(d) shows the local diffusion factor, defined on a streamline from rotor inlet to exit

$$D = 1 - \frac{W_{\text{out}}}{W_{\text{in}}} + \frac{|r_{\text{out}} W_{\theta\text{out}} - r_{\text{in}} W_{\theta\text{in}}|}{W_{\text{in}}} \frac{2\pi/B}{c_{\text{ref}}} \quad (12)$$

where c_{ref} is a reference chord length and B is the number of blades or vanes. The nonaxisymmetric throughflow analysis captures two effects linked to experimentally observed changes in local rotor blade performance. First, the large streamtube contraction near midspan at $\theta = 180$ deg results in a local decrease in diffusion factor, even with large flow turning (at E). Second, the circumferential nonuniformity in diffusion factor is largest near the tip, and the peak diffusion factor in the tip region occurs to the left of the $\theta = 180$ deg position (at F). In the actual flow, this increased loading results in a separation that continues around a large portion of the annulus [14]. The nonaxisymmetric throughflow analysis does not resolve this feature, but the circumferential variations in diffusion factor are consistent with experimental results, and regions of peak diffusion factor are indicators of the potential separation locations in the actual flow. The magnitude of the diffusion factor circumferential distortion is therefore used in Sec. 4 as a metric to characterize nonuniformity in local blade conditions.

3.4 Stator Flow Field. Figure 9 shows a comparison of calculated and measured circumferential distributions of stator inlet (station 4) axial velocity and absolute swirl angle, at 25% and 75% span. The calculated axial velocity distortion is in good agreement with the measurements. Comparison with Fig. 7 shows that both radial and circumferential variations in axial velocity are smaller at rotor exit than at rotor inlet. The swirl angle distributions also agree with the data, but the absolute swirl magnitudes are overestimated by approximately 5 deg, consistent with the slight overprediction of the design point stage loading coefficient in Fig. 4. The agreement with experimental measurements in Figs. 7 and 9 demonstrates that the nonaxisymmetric throughflow analysis (i) captures the important aspects of the three-dimensional flow redistribution and rotor distortion response and (ii) can be used to determine the magnitude of circumferential flow nonuniformities in the rotor and stator with BLI.

Figure 10 shows the distributions of stator inlet stagnation pressure, axial velocity, swirl angle, and stator diffusion factor. The stagnation pressure distribution (Fig. 10(a)) results from

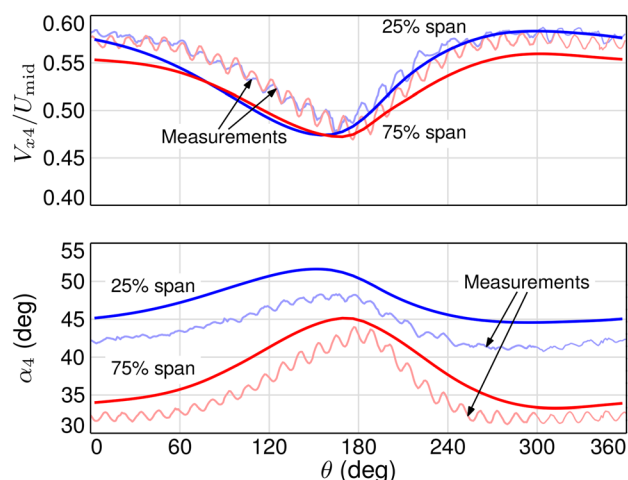


Fig. 9 Circumferential distributions of stator inlet axial velocity and absolute swirl angle; comparison of nonaxisymmetric throughflow calculation and measurements [14]

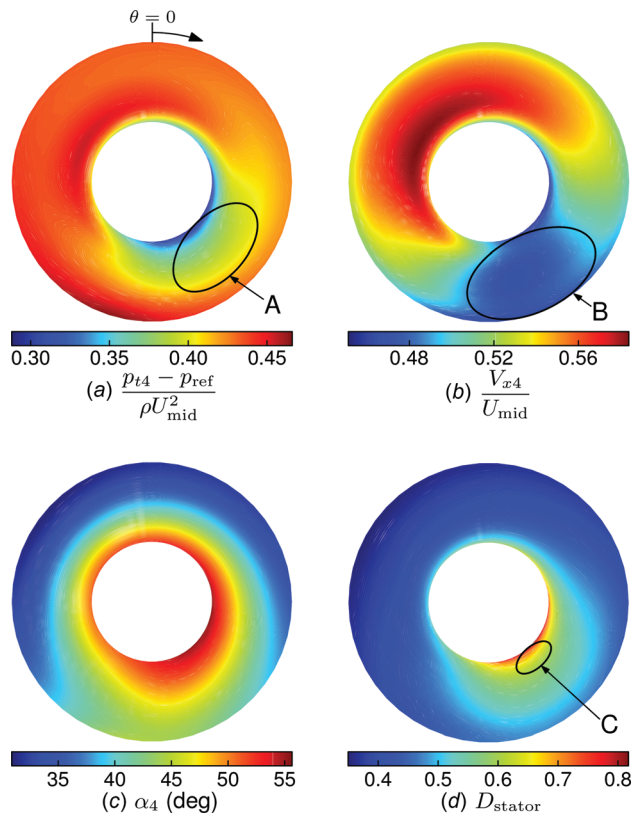


Fig. 10 Calculated stator inlet stagnation pressure (a), inlet axial velocity (b), inlet absolute swirl angle (c), and diffusion factor (d)

combination of the far upstream inlet distortion and the nonuniform work input (Fig. 8(b)). The smallest circumferential variation in stagnation pressure is near the tip, where the nonuniformity in rotor work input is large. At midspan, there is low stagnation pressure to the right of $\theta = 180$ deg (at A) where the incoming stagnation pressure is low and the rotor pressure rise is reduced due to coswirl. The largest circumferential variation in stagnation pressure is near the hub, where, even though the upstream distortion is low, the variation in rotor incidence, and thus nonuniformity in rotor pressure rise, is large. This may be of concern for downstream compressors which ingest the rotor exit hub flow, although that issue is beyond the scope of this paper.

The rotor exit axial velocity distortion (Fig. 10(b)) is less severe than that at rotor inlet. The lowest axial velocities occur to the right of $\theta = 180$ deg (at B), where upstream velocity is low, and pressure rise and distortion attenuation through the rotor are reduced due to coswirl. The rotor relative exit flow is approximately uniform, so the absolute swirl angle, shown in Fig. 10(c), is increased in the region of decreased axial velocity.

The largest effect on stator diffusion factor (Fig. 10(d)) is that of flow turning. The diffusion factor is increased in the region of decreased axial velocity, where the incoming swirl angle is largest. The peak diffusion factor and the largest circumferential variation in diffusion factor both occur near the hub, consistent with experimental observations of increased loading leading to hub corner separation near the location of highest diffusion (at C) [14]. Again, the nonaxisymmetric throughflow analysis does not directly address separation, but circumferential variation in diffusion factor is a predictor of potential regions of increased blade loss.

4 Effect of Turbomachinery Design

We now assess the effect of stage design features on the distortion flow mechanisms described above, and their potential impact

on fan performance, by examining circumferential flow nonuniformities for a range of fan stage designs.

4.1 Parametric Stage Design Description. The fan stages examined are based on the NASA R4 fan stage, which has a design pressure ratio (1.47) and hub-to-tip ratio (0.3) representative of contemporary fan stages. The performance with uniform inlet conditions is documented in Ref. [25]. A meridional view of the computational domain, including three stator axial locations, is given in Fig. 11. The mesh topology, boundary conditions, and calculation procedures as described above for the Whittle Laboratory BLI fan rig geometry were used.

The impact of (i) stage design point flow coefficient and stagnation enthalpy rise coefficient, (ii) radial distribution of stagnation enthalpy rise, (iii) axial location of the downstream stator, and (iv) nonaxisymmetric stator exit flow angle were examined. Table 2 lists the relevant rotor and stator design parameters considered for the geometries assessed. Cells shaded red and blue indicate values greater than and less than the baseline design (case 0), respectively. Darker shading indicates larger relative changes.

Different rotor design points with radially uniform stagnation enthalpy rise are compared to assess the effect of pressure rise characteristic slope, which increases in steepness with decreasing ϕ and ψ . Different radial work distributions at fixed stage stagnation enthalpy rise and flow coefficient are compared to assess the effect of local variations in rotor loading. All the designs have constant ψ/ϕ^2 , representing the condition of constant thrust, which is the relevant comparison. The rotor camber normal distributions were generated by fixing the inlet metal angle distribution for zero incidence based on design point flow coefficient, using circular arc camber distributions at a given spanwise section, and adjusting the exit metal angle distribution until the desired stagnation enthalpy was achieved.

The baseline stator camber surface was taken as a flat plate with zero stagger (i.e., $\hat{\mathbf{n}} = \hat{\theta}$), because the inviscid distortion response is determined by the stator exit flow angle and is insensitive to the details of the camber line. Different stator axial locations are compared to assess the effect of rotor–stator interaction. Nonaxisymmetric stator geometries are also considered to assess the impact of downstream pressure nonuniformities. Circumferential distortions in stator exit flow angle, and thus static pressure, were generated using a circumferential stator camber surface variation of the form

$$\hat{\mathbf{n}} = -\sin[\delta\gamma \cos(\theta - \theta_\gamma)]\hat{\mathbf{x}} + \cos[\delta\gamma \cos(\theta - \theta_\gamma)]\hat{\theta} \quad (13)$$

where $\delta\gamma$ and θ_γ define the magnitude and phase of the variation in stator exit metal angle.

Table 2 lists the peak-to-peak circumferential variation and circumferential average of diffusion factor for hub (10% span), mid-span (50% span), and tip (90% span) sections in both blade rows for the designs considered. Circumferential variations in diffusion factor have been linked to circumferential variations in efficiency [14], and we assume lower values of ΔD are associated with favorable reduction in blade section operating point excursions away from peak efficiency. The blade and vane counts are fixed at

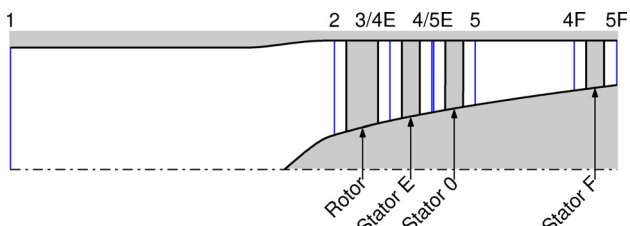


Fig. 11 Meridional geometry of fan stage domain for design sensitivity study, with three axial stator locations shown

Table 2 Stage design and blade row performance for baseline design (0), rotor design variations (A–D), and stator design variations (E–H); cell shading indicates changes relative to the baseline design

		0	A	B	C	D	E	F	G	H	
Stage Design	ϕ	0.47	0.51	0.42	0.47	0.47	0.47	0.47	0.47	0.47	+200%
	ψ	0.24	0.29	0.19	0.24	0.24	0.24	0.24	0.24	0.24	+100%
	ψ_{hub}	0.24	0.29	0.19	0.27	0.20	0.24	0.24	0.24	0.24	0
	ψ_{mid}	0.25	0.29	0.19	0.26	0.23	0.25	0.25	0.25	0.25	-100%
	ψ_{tip}	0.24	0.29	0.19	0.20	0.27	0.24	0.24	0.24	0.24	+100%
	$L_{\text{r-s}}/r_{\text{tip}}$	0.50	0.50	0.50	0.50	0.16	1.5	0.50	0.50	0.50	+200%
	$\delta\gamma$	0	0	0	0	0	0	1.5°	3.0°	3.0°	+100%
	θ_{γ}	-	-	-	-	-	-	180°	270°	270°	0
Rotor Performance	ΔD_{hub}	0.045	0.047	0.046	0.055	0.036	0.034	0.052	0.026	0.066	+200%
	ΔD_{mid}	0.032	0.025	0.052	0.032	0.033	0.020	0.037	0.023	0.041	+100%
	ΔD_{tip}	0.050	0.048	0.051	0.047	0.052	0.046	0.054	0.056	0.027	0
	$D_{\theta-\text{avg},\text{hub}}$	0.27	0.22	0.29	0.22	0.30	0.28	0.27	0.27	0.27	-100%
	$D_{\theta-\text{avg},\text{mid}}$	0.40	0.44	0.33	0.41	0.37	0.39	0.39	0.40	0.39	+200%
	$D_{\theta-\text{avg},\text{tip}}$	0.32	0.36	0.26	0.30	0.33	0.32	0.32	0.32	0.32	+100%
Stator Performance	ΔD_{hub}	0.034	0.023	0.048	0.026	0.043	0.051	0.029	0.057	0.082	+200%
	ΔD_{mid}	0.039	0.034	0.049	0.038	0.038	0.064	0.014	0.068	0.088	+100%
	ΔD_{tip}	0.043	0.039	0.049	0.055	0.036	0.076	0.013	0.076	0.096	0
	$D_{\theta-\text{avg},\text{hub}}$	0.39	0.44	0.33	0.39	0.37	0.48	0.16	0.39	0.39	-100%
	$D_{\theta-\text{avg},\text{mid}}$	0.28	0.31	0.23	0.27	0.26	0.33	0.12	0.28	0.27	+200%
	$D_{\theta-\text{avg},\text{tip}}$	0.22	0.25	0.18	0.21	0.22	0.26	0.10	0.22	0.22	+100%

22 and 54, respectively, and the circumferential average, $D_{\theta-\text{avg}}$ represents the blade section diffusion at peak efficiency.

4.2 Rotor Design Variations. Designs A and B in Table 2 have design point stagnation enthalpy rise values 20% greater than and less than the baseline design, respectively, and a radial distribution of stagnation enthalpy rise that is approximately uniform. Designs C and D have approximately linear radial variations in stagnation enthalpy rise at overall flow and stagnation enthalpy rise coefficients that are the same as the baseline design. The main findings are as follows: (i) Increasing stage flow and stagnation enthalpy rise coefficients decreases rotor midspan diffusion factor distortion with little effect near hub and tip. (ii) Local increases in stagnation enthalpy rise for a given stage design point increase local rotor diffusion factor distortion. (iii) Local increases in stagnation enthalpy rise coefficient decrease local stator diffusion distortion.

The largest change in rotor diffusion nonuniformity occurs at the midspan, where the dominant effect is the nonuniform streamtube contraction (region D of Fig. 8(d)). Increased loading results in a 22% reduction, and decreased loading results in a 16% increase, in diffusion factor distortion. Figure 12 shows the circumferential distributions of streamtube contraction and diffusion factor for designs 0, A, and B at rotor midspan. Higher stagnation enthalpy rise yields more uniform streamtube contraction, and thus enables smaller circumferential variations in diffusion at higher average diffusion factor. This decrease in flow nonuniformity at higher flow and stagnation enthalpy rise coefficient is opposite to behavior expected from *parallel compressor theory*, in which such designs have shallow pressure rise characteristic slope in a way consistent with two-dimensional parallel compressor theory [9]. As such, the behavior illustrates the importance of three-dimensional redistribution.

The midspan diffusion factor distortion is unaffected by radial stagnation enthalpy rise variations at fixed overall stage flow and stagnation rise enthalpy coefficient (designs 0, C, and D). Near the hub and tip, on the other hand, diffusion factor nonuniformity increases with increased local stagnation enthalpy rise. These results indicate (i) the three-dimensional redistribution is

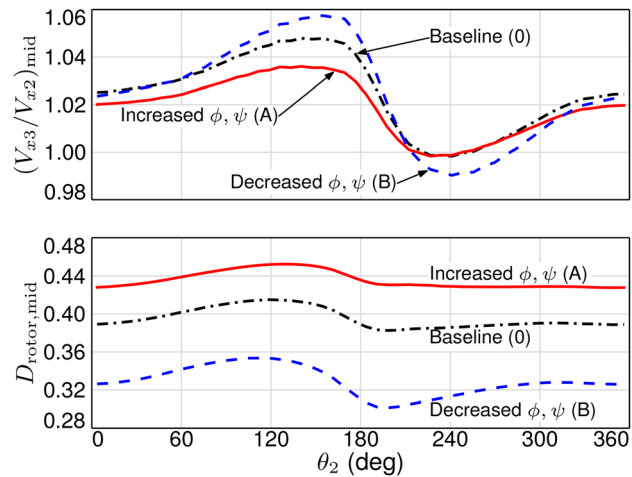


Fig. 12 Circumferential distributions of rotor streamtube contraction and diffusion factor at 50% span for baseline (0), increased (A), and decreased (B) flow and stagnation enthalpy rise coefficient designs

governed by the overall stage flow and stagnation enthalpy rise coefficients, as described above, and (ii) the rotor spanwise section performance changes with local pressure rise characteristic slope in a way consistent with two-dimensional parallel compressor theory.

For all rotor designs, the nonuniformity in stator diffusion is increased as local rotor stagnation enthalpy rise coefficient is reduced, although the effect is smaller than for the rotor midspan diffusion factor distortions just described. The local stator diffusion is determined by the rotor exit axial velocity; with the nearly constant rotor relative exit angle, smaller axial velocity gives larger turning, and thus higher diffusion, in the stator. The increase in stator diffusion distortion with lower loading is thus a

consequence of reduced attenuation of axial velocity distortion through the rotor.

4.3 Stator Design Variations. Designs E and F in Table 2 have the closely spaced and far-spaced stator rows, respectively, shown in Fig. 11. Designs G and H have nonaxisymmetric stator designs that were found to reduce rotor diffusion factor distortion locally near the hub and tip, respectively. The main findings are as follows: (i) Changes in stator design have a larger effect than the rotor work distribution on reducing diffusion factor distortion in either the rotor or stator. (ii) Decreasing rotor–stator spacing decreases rotor flow distortions while increasing stator flow distortions. (iii) Circumferential variations in stator exit angle distributions give improvements in rotor diffusion factor over a portion of the span only while increasing stator distortion over the entire span.

The rotor diffusion distortion reduction is achieved through a favorable rotor exit pressure due to interaction between the rotor exit distortion and the downstream stator. For a circumferentially uniform exit static pressure, the local stator pressure rise will be higher where the rotor exit stagnation pressure is low and absolute swirl angle is high. This effect is illustrated in Fig. 13, which shows circumferential distributions, at 90% span, of rotor exit static pressure and rotor diffusion factor for designs 0, E, and H. The closely spaced stator has reduced rotor exit pressure, relative to the baseline design, where the diffusion factor is highest, yielding an 8% reduction in rotor diffusion factor distortion. Nonuniform stator exit flow angles also modify the rotor exit pressure by introducing stator exit static pressure nonuniformity. Design H thus reduces the rotor diffusion factor distortion by 46% relative to the baseline design.

The reduction in rotor diffusion factor distortion occurs in part because of reduced attenuation of the upstream stagnation pressure distortion, resulting in increased axial velocity distortion downstream of the rotor and increased stator diffusion factor distortion. For the geometry considered here, the stator distortion is also affected by the favorable pressure gradient due to area contraction downstream of the rotor; increased spacing reduces the distortion upstream of the stator. For the nonaxisymmetric stator designs, the stator distortion is increased due to the downstream flow angle distortion.

4.4 Discussion: Design Features for BLI Fans. To help organize the above results, it is useful to discuss fan stage attributes for mitigating the effect of BLI inlet distortion, based on a metric of reduction in diffusion factor nonuniformity. Although

we do not address the point further, such reductions can lessen the unsteady forces on the rotor and the magnitude and duration of locally increased loading, which may impact stall margin [21]. Further analysis with higher-fidelity tools is necessary to assess the effectiveness of the suggested design features.

4.4.1 Nonaxisymmetric Stator Geometry. Changes in the rotor exit static pressure field from nonaxisymmetric stator exit flow angle were found to have the largest effect on rotor diffusion factor variation. Nonaxisymmetric stator geometries have been used to mitigate the effect of flow nonuniformities due to downstream components (e.g., pylons) [26,27], and they appear to be well suited to mitigate the effect of upstream nonuniformities due to BLI. Only two-dimensional circumferential variations in stator exit metal angle, as described in Eq. (13), have been considered here. Different combinations of stator exit angle magnitude and phase produced reductions in rotor diffusion distortion at different spanwise locations. A stator exit angle distribution with both radial and circumferential variations could be designed to generate a rotor exit pressure field that reduces rotor flow distortions over larger portions of the span. Such designs would reduce the rotor distortion attenuation and thus yield larger flow angle variations at the stator inlet, but the impact of this could be mitigated through nonaxisymmetric tailoring of the stator leading edge to match the upstream flow angle. Nonaxisymmetric stator geometry thus shows promise as a means to mitigate BLI flow distortions to improve performance in both the rotor and stator.

4.4.2 Reduced Rotor–Stator Axial Spacing. The rotor exit distortion results in nonuniform stator loading and thus a nonuniform stator inlet static pressure field aligned with the stagnation pressure distortion. This provides a rotor exit pressure that accelerates high diffusion streamtubes more strongly than those with low diffusion, alleviating diffusion nonuniformities. This effect, and the upstream influence of nonaxisymmetric stator exit flow angle (described above), becomes stronger as the axial distance between the rotor and stator decreases. Fan exit guide vanes located less than a tip radius downstream of the rotor trailing edge could thus enable gains in BLI fan rotor performance relative to designs where the stator is far downstream and does not interact with the rotor.

4.4.3 Flow and Stagnation Enthalpy Rise Coefficients. The analysis in Sec. 3 shows the importance of both circumferential and radial flow redistribution in BLI fans. The results in Table 2 indicate that the upstream redistribution depends on the overall stage flow coefficient and pressure rise. Designs with low flow coefficient and low stagnation enthalpy rise coefficient have steep pressure rise versus flow coefficient characteristics, leading to stronger upstream redistribution and increased rotor inlet co- and counterswirl. This, in turn, results in increased nonuniformities in stagnation enthalpy rise and streamtube contraction. For the rotor designs examined, the largest decrease in rotor diffusion factor distortion occurred at midspan for the high flow and stagnation enthalpy rise coefficient (shallow characteristic) design, and thus due to a reduction in streamtube contraction nonuniformity. The implication is that *reduction in distortion attenuation may enable reduced losses within the propulsor*. Such designs are consistent with trends in modern fans toward lower tip speeds and higher corrected flow per unit area, but come at the cost of increased average diffusion in both blade rows and increased flow nonuniformity in the jet. These trades need to be investigated for BLI propulsion systems.

4.4.4 Radial Loading Distribution. For a given stage design (stagnation enthalpy rise and flow coefficient), the three-dimensional flow redistribution is not sensitive to changes in the radial loading distribution. The local blade row response to changes in loading is similar to that in two-dimensional flows [4,9]; increased loading leads to increased nonuniformity in the rotor and decreased nonuniformity in the stator. This feature may

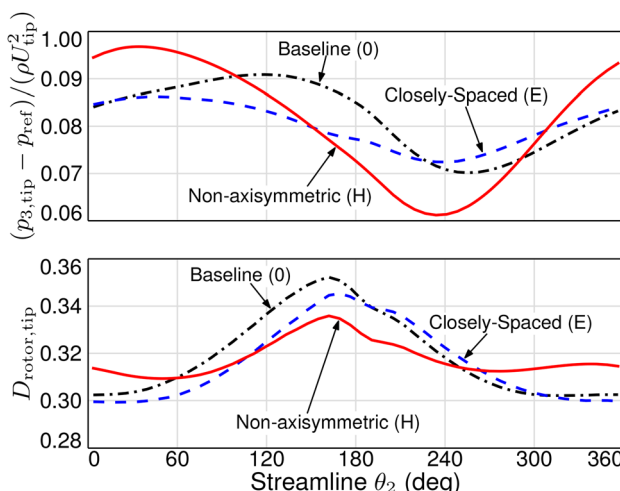


Fig. 13 Circumferential distributions of rotor exit static pressure and diffusion factor at 90% span for baseline (0), closely spaced (E), and nonaxisymmetric (H) stator designs

be useful in addressing local circumferential nonuniformities, for example, reducing the rotor tip loading, because nonuniformities in the tip region have been linked to reduction in fan stall margin [21]. Improvements in one performance at one spanwise section appear to worsen the performance at another location, however, and clear links between axisymmetric rotor loading distribution and overall performance improvements with BLI distortion are not yet defined.

5 Summary and Conclusions

A new nonaxisymmetric throughflow analysis has been developed to evaluate, at the conceptual level, i.e., without the blade geometry, the response of fan stages to BLI inlet distortion. The turbomachinery is modeled using momentum and energy source distributions that are a function of local flow conditions and a blade mean camber surface. The analysis, which allows the estimation of flow fields using steady CFD methods, has been compared to experimental data and high-fidelity computations and shown to effectively capture the principal features of fan response to BLI distortion.

Using the nonaxisymmetric throughflow analysis, the impact of BLI inlet distortion on fan stage flow fields has been assessed. The results illustrate the importance of flow redistribution effects upstream and through the rotor. Some aspects of the distortion attenuation can be explained using ideas from two-dimensional distortion analysis, but the analysis shows that a three-dimensional description is required to define the redistribution and the interactions between spanwise stations.

The effect of (i) design flow and stagnation enthalpy rise coefficients, (ii) radial distribution of work input, (iii) rotor–stator spacing, and (iv) nonaxisymmetric stator exit flow angle on circumferential variations in blade row diffusion has been assessed. Increasing stage flow coefficient and stagnation enthalpy rise coefficient results in decreased distortion in both the rotor and stator. Varying radial work distribution results in trades between distortions in the rotor and stator or between spanwise sections of a given blade row. The nonuniform stator loading induced by the rotor exit distortion produces a favorable rotor exit pressure. Reducing axial spacing between the rotor and stator thus results in reduced rotor flow distortion. Nonaxisymmetric stator exit angles may be used to improve the favorable rotor exit pressure and reduce rotor flow distortions further. Reduction in the rotor flow distortion implies a reduction in distortion attenuation and thus an increase in stator inlet distortion, the effect of which can be mitigated with a nonuniform stator leading edge metal angle distribution designed to accept the incoming distortion. Of the several approaches examined, therefore, nonaxisymmetric stator design therefore appears to be best suited to improving BLI fan performance.

Acknowledgment

This research was supported by the NASA Fundamental Aeronautics Program, Fixed Wing Project, at the NASA Glenn Research Center under Cooperative Agreement No. NNX11AB35A and the MIT-SUTD Graduate Fellows Program. The authors would also like to acknowledge E. J. Gunn, D. Perovic, and C. A. Hall of the Whittle Lab for information about their rig and measurements, and E. Envia of NASA for information on the R4 fan stage. Thanks also to J. J. Defoe, C. Lettieri, W. A. Sorensen, A. P. Kottapalli, M. L. Brand, and A. Peters for useful conversations during the development of the source term model, and M. Drela, N. A. Cumpsty, Z. S. Spakovszky, and A. Uranga for their helpful comments and suggestions.

Nomenclature

A = area
 \bar{A} = blade aspect ratio

B	= number of blades
c	= chord length
c_ℓ	= two-dimensional airfoil lift coefficient
D	= diffusion factor
\dot{e}	= specific energy source term
\mathbf{f}	= specific momentum source vector
h_t	= stagnation enthalpy
L_{r-s}	= rotor–stator axial spacing
\dot{m}	= mass flow
$\hat{\mathbf{n}}$	= blade camber surface normal
p, p_t	= static, stagnation pressure
s	= entropy, blade pitch
V	= velocity magnitude
\mathbf{V}	= velocity vector
U	= wheel speed (Ωr)
W	= blade-relative velocity magnitude
\mathbf{W}	= blade-relative velocity vector ($\mathbf{V} - (\Omega r)\hat{\theta}$)
x, r, θ	= cylindrical coordinate axes
x, y, z	= Cartesian coordinate axes

Greek Symbols

α	= absolute swirl angle
β	= reduced frequency, blade-relative swirl angle
γ	= stagger angle
δ	= local relative flow deviation angle
$\delta\gamma$	= stator stagger angle nonuniformity magnitude
ΔD	= circumferential variation in diffusion factor
θ_γ	= stator stagger angle nonuniformity phase
ρ	= density
ϕ	= flow coefficient (V_{x2}/U_{tip})
ψ	= stagnation enthalpy rise coefficient $((h_{t3} - h_{t2})/U_{tip}^2)$
Ω	= rotor angular velocity

Subscripts

hub	= blade hub (10% span)
in	= blade row inlet
mid	= blade midspan (50% span)
out	= blade row outlet
ref	= reference value
tip	= blade tip (90% span)
1	= far upstream measurement location
2	= rotor inlet plane measurement location
3	= rotor exit measurement location
4	= stator inlet measurement location
5	= stator exit measurement location
θ -avg	= circumferential average

References

- [1] Betz, A., 1966, *Introduction to the Theory of Flow Machines*, Pergamon Press, New York.
- [2] Smith, L. H., 1993, "Wake Ingestion Propulsion Benefit," *AIAA J. Propul. Power*, **9**(1), pp. 74–82.
- [3] Sato, S., 2012, "The Power Balance Method for Aerodynamic Performance Assessment," *Ph.D. dissertation*, Massachusetts Institute of Technology, Cambridge, MA.
- [4] Hall, D. K., 2015, "Analysis of Civil Aircraft Propulsors With Boundary Layer Ingestion," *Ph.D. dissertation*, Massachusetts Institute of Technology, Cambridge, MA.
- [5] Hall, C. A., Schwartz, E., and Hileman, J. I., 2009, "Assessment of Technologies for the Silent Aircraft Initiative," *AIAA J. Propul. Power*, **25**(6), pp. 1153–1162.
- [6] Greitzer, E. M., Bonnefoy, P. A., De la Rosa Blanco, E., Dorbian, C. S., Drela, M., Hall, D. K., Hansman, R. J., Hileman, J. I., Liebeck, R. H., Lovergren, J., Mody, P., Pertuze, J. A., Sato, S., Spakovszky, Z. S., Tan, C. S., Hollman, J. S., Duda, J. E., Fitzgerald, N., Houghton, J., Kerrebrock, J. L., Kiwada, G. F., Korodonowy, D., Parrish, J. C., Tylko, J., and Wen, E. A., 2010, "N+3 Aircraft Concept Designs and Trade Studies, Final Report," NASA, Washington, DC, Report No. *NASA CR-2010-216794*.
- [7] Drela, M., 2011, "Development of the D8 Transport Configuration," *AIAA Paper No. 2011-3970*.
- [8] Uranga, A., Drela, M., Greitzer, E. M., Titchener, N. A., Lieu, M. K., Siu, N. M., Huang, A. C., Gatlin, G. M., and Hannon, J. A., 2014, "Preliminary

- Experimental Assessment of the Boundary Layer Ingestion Benefit for the D8 Aircraft," *AIAA* Paper No. 2014-0906.
- [9] Longley, J. P., and Greitzer, E. M., 1992, "Inlet Distortion Effects in Aircraft Propulsion System Integration," *Steady and Transient Performance Prediction of Gas Turbine Engines* (AGARD Lecture Series, Vol. 183), Advisory Group for Aerospace Research and Development, Neuilly sur Seine, France.
- [10] Greitzer, E. M., and Griswold, H. R., 1976, "Compressor-Diffuser Interaction With Circumferential Flow Distortion," *J. Mech. Eng. Sci.*, **18**(1), pp. 25–38.
- [11] Hynes, T. P., and Greitzer, E. M., "A Method for Assessing Effects of Circumferential Flow Distortion on Compressor Stability," *ASME J. Turbomach.*, **109**(3), pp. 371–379.
- [12] Florea, R. V., Matalanis, C., Hardin, L. W., Stucky, M., and Shabbir, A., 2015, "Parametric Analysis and Design for Embedded Engine Inlets," *AIAA J. Propul. Power*, **31**(3), pp. 843–850.
- [13] Gunn, E. J., Tooze, S. E., Hall, C. A., and Colin, Y., 2013, "An Experimental Study of Loss Sources in a Fan Operating With Continuous Inlet Stagnation Pressure Distortion," *ASME J. Turbomach.*, **135**(5), p. 051002.
- [14] Gunn, E. J., and Hall, C. A., 2014, "Aerodynamics of Boundary Layer Ingesting Fans," *ASME* Paper No. GT2014-26142.
- [15] Defoe, J. J., and Hall, D. K., 2016, "Fan Performance Scaling With Inlet Distortions," *ASME* Paper No. GT2016-58009.
- [16] Marble, F., 1964, "Three-Dimensional Flow in Turbomachines," *High Speed Aerodynamics and Jet Propulsion*, W. R. Hawthorne, ed., Princeton University Press, Princeton, NJ, pp. 83–166.
- [17] Gong, Y., Tan, C. S., Gordon, K. A., and Greitzer, E. M., 1999, "A Computational Model for Short-Wavelength Stall Inception and Development in Multi-stage Compressors," *ASME J. Turbomach.*, **121**(4), pp. 726–734.
- [18] Peters, A., Spakovszky, Z. S., Lord, W. K., and Rose, B., 2015, "Ultrashort Nacelles for Low Fan Pressure Ratio Propulsors," *ASME J. Turbomach.*, **137**(2), p. 021001.
- [19] Defoe, J. J., and Spakovszky, Z. S., 2013, "Effects of Boundary-Layer Ingestion on the Aero-Acoustics of Transonic Fan Rotors," *ASME J. Turbomach.*, **135**(5), p. 051013.
- [20] Horlock, J. H., 1971, "On Entropy Production in Adiabatic Flow in Turbomachines," *ASME J. Basic Eng.*, **93**(4), pp. 587–593.
- [21] Perovic, D., Hall, C. A., and Gunn, E. J., 2015, "Stall Inception in a Boundary Layer Ingesting Fan," *ASME* Paper No. GT2015-43025.
- [22] Hall, C. A., 2015, personal communication.
- [23] Pointwise, 2015, "Pointwise®: User Manual," Release 17, Pointwise, Inc., Fort Worth, TX.
- [24] ANSYS, 2013, "ANSYS® CFX-Solver Theory Guide," Release 15.0, ANSYS, Inc., Canonsburg, PA.
- [25] Hughes, C. E., 2002, "Aerodynamic Performance of Scale-Model Turbofan Outlet Guide Vanes Designed for Low Noise," *AIAA* Paper No. 2002-0374.
- [26] Kodama, H., and Nagano, S., 1987, "Potential Pressure Field by Stator/Downstream Strut Interaction," *ASME J. Turbomach.*, **111**(2), pp. 197–203.
- [27] Parry, A. B., 1996, "Optimisation of Bypass Fan Outlet Guide Vanes," *ASME* Paper No. 96-GT-433.